Electronic Supporting Information for:

Broadband Yellow and White Emission from Large Octahedral Tilting in (110)-Oriented Layered Perovskites: Imidazolium-Methylhydrazinium Lead Halides

Authors: Dawid Drozdowski,*[,a] Katarzyna Fedoruk,[b] Adam Kabański,[a] Adam Sieradzki,[b]

Mirosław Mączka[a] and Anna Gągor*[,a]

[a]*Institute of Low Temperature and Structure Research, Polish Academy of Sciences, ul. Okólna 2, 50-422 Wrocław, Poland*
[b]*Department of Experimental Physics, Wrocław University of Science and Technology, Wybrzeże Wyspiańskiego 27, 50-370 Wrocław, Poland*

* - Corresponding Authors; e-mails: d.drozdowski@intibs.pl, a.gagor@intibs.pl

Table S1. Experimental and refinement details of IMMHyPbBr$_4$ (IMPB, M_r = 643.01).

	Phase I, 358 K	Phase II, 295 K	Phase II, 100 K
Crystal data			
Crystal system, space group	Monoclinic, $P2/c$	Monoclinic, $P2_1/c$	Monoclinic, $P2_1/c$
Temperature (K)	358	295	100
a, b, c (Å)	6.0384 (4), 13.970 (1), 8.5113 (6)	5.9753 (7), 28.414 (4), 8.2762 (12)	5.9431 (2), 28.182 (1), 8.1723 (4)
β (°)	92.06 (1)	90.49 (1)	91.129 (3)
V (Å^3)	717.53 (8)	1405.1 (3)	1368.5 (1)
Z	2	4	4
μ (mm^{-1})	22.86	23.35	24.12
Crystal size (mm)	0.2 × 0.14 × 0.07	0.2 × 0.14 × 0.07	0.35 × 0.17 × 0.11
Data collection			
T_{min}, T_{max}	0.106, 1.000	0.280, 1.000	0.219, 1.000
No. of measured, independent and observed [$I > 2\sigma(I)$] reflections	4566, 1480, 1198	6467, 2846, 2188	13903, 2798, 2594
R_{int}	0.032	0.042	0.048
$(\sin \theta/\lambda)_{max}$ (Å^{-1})	0.625	0.625	0.625
Refinement			
$R[F^2 > 2\sigma(F^2)]$, $wR(F^2)$, S	0.044, 0.115, 1.02	0.057, 0.124, 1.09	0.039, 0.090, 1.17
No. of reflections	1480	2846	2798
No. of parameters	59	114	84
No. of restraints	9	0	6
$\Delta\rho_{max}$, $\Delta\rho_{min}$ (e Å^{-3})	1.89, -1.56	1.59, -2.39	2.36, -2.75

Table S2. Experimental and refinement details of IMMHyPbCl$_4$ (IMPC, M_r = 465.17)

	Phase I, 390 K	Phase II, 295 K	Phase II, 100 K
Crystal data			
Crystal system, space group	Monoclinic, $P2/c$	Monoclinic, $P2_1/c$	Monoclinic, $P2_1/c$
Temperature (K)	390	295	100
a, b, c (Å)	5.7615 (4), 13.725 (1), 8.1876 (9)	5.7168 (2), 27.883 (1), 8.0079 (3)	5.6652 (2), 27.388 (2), 7.9492 (4)
β (°)	90.47 (1)	90.132 (3)	90.453 (4)
V (Å^3)	647.4 (1)	1276.45 (8)	1233.3 (1)
Z	2	4	4
μ (mm^{-1})	13.82	14.02	14.51
Crystal size (mm)	0.15 × 0.11 × 0.02	0.15 × 0.11 × 0.02	0.24 × 0.12 × 0.04
Data collection			
T_{min}, T_{max}	0.145, 1.000	0.362, 1.000	0.201, 1.000
No. of measured, independent and observed [$I > 2\sigma(I)$] reflections	2397, 1093, 874	25547, 2585, 2380	13157, 2508, 2351
R_{int}	0.046	0.038	0.034
$(\sin\theta/\lambda)_{max}$ (Å^{-1})	0.609	0.625	0.625
Refinement			
$R[F^2 > 2\sigma(F^2)]$, $wR(F^2)$, S	0.047, 0.112, 1.04	0.029, 0.062, 1.24	0.029, 0.071, 1.16
No. of reflections	1093	2585	2508
No. of parameters	59	114	120
No. of restraints	9	0	0
$\Delta\rho_{max}$, $\Delta\rho_{min}$ (e Å^{-3})	0.83, -1.16	1.24, -2.04	1.30, -1.78

Table S3. Selected geometric parameters of IMPB (Å, º)

Phase I, 358 K			
Pb1—Br1	3.0198 (2)	Pb1—Br2	3.108 (7)
Pb1—Br1^i	3.0198 (2)	Pb1—Br2^{iii}	3.110 (7)
Pb1—Br3	2.8983 (12)	Pb1—Br2^{ii}	3.108 (7)
Pb1—Br3^{ii}	2.8983 (12)	Pb1—Br2^{iv}	3.110 (7)
Br1—Pb1—Br1^i	177.78 (8)	Br3—Pb1—Br3^{ii}	92.20 (8)
Br1—Pb1—Br2^{iii}	87.77 (17)	Br3—Pb1—Br2^{iii}	94.85 (17)
Br1—Pb1—Br2^{iv}	93.95 (17)	Br3^{ii}—Pb1—Br2^{iv}	94.85 (17)
Br1—Pb1—Br2^{ii}	84.81 (17)	Br3^{ii}—Pb1—Br2^{ii}	85.96 (17)
Br1^i—Pb1—Br2^{iii}	93.96 (17)	Br3^{ii}—Pb1—Br2^{iii}	172.37 (11)
Br1^i—Pb1—Br2^{ii}	96.67 (17)	Br3—Pb1—Br2^{ii}	173.57 (13)
Br1^i—Pb1—Br2^{iv}	87.77 (17)	Br3^{ii}—Pb1—Br2	173.57 (13)
Br1—Pb1—Br2	96.67 (17)	Br3—Pb1—Br2	85.96 (17)
Br1^i—Pb1—Br2	84.81 (17)	Br3—Pb1—Br2^{iv}	172.37 (11)
Br3^{ii}—Pb1—Br1	89.45 (5)	Br2—Pb1—Br2^{iii}	12.71 (13)
Br3^{ii}—Pb1—Br1^i	89.01 (5)	Br2^{ii}—Pb1—Br2^{iii}	86.72 (4)
Br3—Pb1—Br1	89.01 (5)	Br2—Pb1—Br2^{iv}	86.72 (4)
Br3—Pb1—Br1^i	89.45 (5)		
Phase II, 295 K			
Pb1—Br1	2.9821 (16)	Pb1—Br3	3.0134 (16)
Pb1—Br2	2.8697 (16)	Pb1—Br4	2.9909 (15)
Pb1—Br3^v	3.1661 (17)	Pb1—Br4^{vi}	2.9972 (15)
Br1—Pb1—Br3	179.03 (5)	Br2—Pb1—Br4^{vi}	87.24 (5)
Br1—Pb1—Br3^v	94.22 (5)	Br3—Pb1—Br3^v	86.621 (19)
Br1—Pb1—Br4	87.33 (5)	Br4—Pb1—Br3^v	93.11 (5)
Br1—Pb1—Br4^{vi}	89.03 (6)	Br4^{vi}—Pb1—Br3	91.40 (6)
Br2—Pb1—Br1	91.30 (5)	Br4^{vi}—Pb1—Br3^v	93.69 (5)
Br2—Pb1—Br3	87.86 (5)	Br4—Pb1—Br3	92.13 (6)
Br2—Pb1—Br3^v	174.42 (5)	Br4—Pb1—Br4^{vi}	172.51 (7)
Br2—Pb1—Br4	86.30 (5)	Pb1—Br3—Pb1^{vii}	157.79 (7)
Phase II, 100 K			
Pb1—Br1	3.0056 (10)	Pb1—Br3	2.9764 (10)
Pb1—Br2	2.8469 (10)	Pb1—Br4^{vi}	3.0449 (10)
Pb1—Br3^v	3.2135 (10)	Pb1—Br4	2.9500 (10)
Br1—Pb1—Br3^v	93.91 (3)	Br3—Pb1—Br4^{vi}	98.38 (3)
Br1—Pb1—Br4^{vi}	85.00 (3)	Br4—Pb1—Br1	84.02 (3)
Br2—Pb1—Br1	91.25 (3)	Br4—Pb1—Br3^v	91.25 (3)
Br2—Pb1—Br3	86.75 (3)	Br4—Pb1—Br3	92.23 (3)
Br2—Pb1—Br3^v	173.40 (3)	Br4^{vi}—Pb1—Br3^v	99.79 (3)

Br2—Pb1—Br4	85.20 (3)	Br4—Pb1—Br4^{vi}	164.92 (4)
Br2—Pb1—Br4^{vi}	84.74 (3)	Pb1—Br3—Pb1^{vii}	147.54 (4)
Br3—Pb1—Br1	175.89 (3)	Pb1—Br4—Pb1^{viii}	164.92 (4)
Br3—Pb1—Br3^{v}	87.839 (14)		

Symmetry code(s): (i) *x*-1, *y*, *z*; (ii) -*x*, *y*, -*z*+1/2; (iii) -*x*, -*y*+1, -*z*+1; (iv) *x*, -*y*+1, *z*-1/2; (v) *x*, -*y*+1/2, *z*+1/2; (vi) *x*+1, *y*, *z*; (vii) *x*, -*y*+1/2, *z*-1/2, (viii) *x*-1, *y*, *z*.

Table S4. Selected geometric parameters of IMPC (Å, º)

Phase I, 390 K			
Pb1—Cl1	2.8844 (4)	Pb1—Cl2^{iii}	2.98 (4)
Pb1—Cl1^{i}	2.8844 (4)	Pb1—Cl2^{ii}	2.99 (4)
Pb1—Cl3	2.755 (4)	Pb1—Cl2^{iv}	2.98 (4)
Pb1—Cl3^{ii}	2.755 (4)	Pb1—Cl2	2.99 (4)
Br1—Pb1—Br1^{i}	177.78 (8)	Br3^{ii}—Pb1—Br2^{iv}	94.85 (17)
Br1—Pb1—Br2^{iii}	87.77 (17)	Br3^{ii}—Pb1—Br2^{ii}	85.96 (17)
Br1—Pb1—Br2^{iv}	93.95 (17)	Br3^{ii}—Pb1—Br2^{iii}	172.37 (11)
Br1—Pb1—Br2^{ii}	84.81 (17)	Br3—Pb1—Br2^{ii}	173.57 (13)
Br1^{i}—Pb1—Br2^{iii}	93.96 (17)	Br3^{ii}—Pb1—Br2	173.57 (13)
Br1^{i}—Pb1—Br2^{ii}	96.67 (17)	Br3—Pb1—Br2	85.96 (17)
Br1^{i}—Pb1—Br2^{iv}	87.77 (17)	Br3—Pb1—Br2^{iv}	172.37 (11)
Br1—Pb1—Br2	96.67 (17)	Br2—Pb1—Br2^{iii}	12.71 (13)
Br1^{i}—Pb1—Br2	84.81 (17)	Br2^{ii}—Pb1—Br2^{iii}	86.72 (4)
Br3^{ii}—Pb1—Br1	89.45 (5)	Br2—Pb1—Br2^{iv}	86.72 (4)
Br3^{ii}—Pb1—Br1^{i}	89.01 (5)	Br2^{iii}—Pb1—Br2^{iv}	78.3 (3)
Br3—Pb1—Br1	89.01 (5)	Br2^{ii}—Pb1—Br2^{iv}	12.71 (13)
Br3—Pb1—Br1^{i}	89.45 (5)	Br2^{ii}—Pb1—Br2	96.5 (3)
Br3—Pb1—Br3^{ii}	92.20 (8)	Pb1^{v}—Br1—Pb1	177.78 (8)
Br3—Pb1—Br2^{iii}	94.85 (17)	Pb1—Br2—Pb1^{iii}	167.29 (13)
Phase II, 295 K			
Pb1—Cl1	2.8911 (19)	Pb1—Cl3^{v}	3.151 (2)
Pb1—Cl2	2.7113 (18)	Pb1—Cl4	2.8625 (18)
Pb1—Cl3	2.852 (2)	Pb1—Cl4^{vi}	2.8882 (18)
Cl1—Pb1—Cl3^{v}	94.48 (6)	Cl3—Pb1—Cl4	93.19 (7)
Cl2—Pb1—Cl1	90.33 (6)	Cl3—Pb1—Cl4^{vi}	93.58 (7)
Cl2—Pb1—Cl3	87.21 (7)	Cl4—Pb1—Cl1	84.85 (7)
Cl2—Pb1—Cl3^{v}	175.12 (6)	Cl4^{vi}—Pb1—Cl1	87.94 (7)
Cl2—Pb1—Cl4	84.61 (6)	Cl4^{vi}—Pb1—Cl3^{v}	95.67 (6)
Cl2—Pb1—Cl4^{vi}	85.30 (6)	Cl4—Pb1—Cl3^{v}	95.00 (6)
Cl3—Pb1—Cl1	176.98 (6)	Cl4—Pb1—Cl4^{vi}	167.55 (9)

Cl3—Pb1—Cl3^v	87.96 (2)	Pb1—Cl4—Pb1^i	167.55 (9)

Phase II, 100 K

Pb1—Cl1	2.8860 (14)	Pb1—Cl3	2.8355 (15)
Pb1—Cl2	2.6755 (15)	Pb1—Cl4^{vi}	2.9552 (14)
Pb1—Cl3^v	3.1971 (16)	Pb1—Cl4	2.7881 (14)
Cl1—Pb1—Cl3^v	93.55 (4)	Cl3—Pb1—Cl4^{vi}	101.62 (4)
Cl1—Pb1—Cl4^{vi}	83.40 (4)	Cl4—Pb1—Cl1	83.00 (4)
Cl2—Pb1—Cl1	90.01 (4)	Cl4—Pb1—Cl3^v	91.79 (4)
Cl2—Pb1—Cl3	86.53 (5)	Cl4—Pb1—Cl3	91.13 (4)
Cl2—Pb1—Cl3^v	174.21 (4)	Cl4^{vi}—Pb1—Cl3^v	102.15 (4)
Cl2—Pb1—Cl4	84.11 (5)	Cl4—Pb1—Cl4^{vi}	161.07 (7)
Cl2—Pb1—Cl4^{vi}	82.78 (4)	Pb1—Cl3—Pb1^{vii}	143.48 (6)
Cl3—Pb1—Cl1	173.47 (4)	Pb1—Cl4—Pb1^i	161.07 (7)
Cl3—Pb1—Cl3^v	89.48 (2)		

Symmetry code(s): (i) x-1, y, z; (ii) -x, y, -z+1/2; (iii) x, -y+1, z-1/2; (iv) -x, -y+1, -z+1; (v) x, -y+1/2, z+1/2; (vi) x+1, y, z; (vii) x, -y+1/2, z-1/2.

Table S5. Selected hydrogen-bond parameters of IMPB in phase **II** at 295 K and 100 K. The N—H···X HBs for MHy$^+$ are marked in red.

D—H···A	D—H (Å)	H···A (Å)	D···A (Å)	D—H···A (°)
Phase II, 295 K				
N4—H4···Br2^i	0.86	2.84	3.506 (18)	135.2
C3—H3···Br1^{ii}	0.93	2.70	3.604 (18)	164.8
N1—H1···N6	0.86	1.99	2.84 (3)	174.4
C2—H2···Br1^{iii}	0.93	2.91	3.74 (2)	149.1
C5—H5···Br2^{iv}	0.93	2.92	3.67 (2)	138.2
Phase II, 100 K				
N4—H4···Br2^i	0.88	2.69	3.356 (9)	133.4
N4—H4···Br4^i	0.88	2.83	3.503 (9)	134.5
C3—H3···Br1^{ii}	0.95	2.83	3.766 (11)	168.2
N1—H1···N6	0.88	2.03	2.904 (12)	174.7
C2—H2···Br1^{iii}	0.95	2.91	3.746 (11)	147.6
C5—H5···Br2^{iv}	0.95	2.82	3.597 (11)	139.9
N6—H6A···Br4	0.88	2.88	3.585 (10)	137.6
N7—H7A···Br1^v	0.91	2.80	3.475 (11)	132.1
N7—H7A···Br4^{iii}	0.91	2.81	3.449 (10)	128.7
N7—H7B···Br1^{iii}	0.91	2.51	3.345 (9)	153.1

Symmetry code(s): (i) -x, -y, -z+1; (ii) -x+1, -y, -z+1; (iii) x, y, z-1; (iv) x-1, y, z; (v) x-1, y, z-1.

Table S6. Selected hydrogen-bond parameters of IMPC in phase **II** at 295 K and 100 K. The N—H⋯X HBs for MHy$^+$ are marked in red.

D—H⋯A	D—H (Å)	H⋯A (Å)	D⋯A (Å)	D—H⋯A (°)
Phase II, 295 K				
N4—H4⋯Cl2^i	0.86	2.68	3.348 (8)	134.9
N4—H4⋯Cl4^i	0.86	2.81	3.491 (8)	137.0
C3—H3⋯Cl1^{ii}	0.93	2.62	3.534 (9)	168.5
N1—H1⋯N6	0.86	1.99	2.840 (11)	169.9
Phase II, 100 K				
C4—H4⋯Cl2^{iii}	0.95	2.77	3.499 (7)	134.5
N3—H3⋯Cl2^i	0.88	2.57	3.233 (5)	132.6
N3—H3⋯Cl4^i	0.88	2.64	3.335 (6)	137.0
N1—H1⋯N6	0.88	1.98	2.857 (8)	173.8
C2—H2⋯Cl1^{ii}	0.95	2.68	3.620 (7)	169.1
C5—H5⋯Cl1^{iv}	0.95	2.81	3.642 (7)	147.3
N6—H6A⋯Cl4	0.86	2.82	3.447 (5)	131.5
N7—H7A⋯Cl1^v	0.91	2.55	3.252 (7)	134.9
N7—H7A⋯Cl4^{iv}	0.91	2.70	3.292 (6)	123.3
N7—H7B⋯Cl1^{iv}	0.91	2.34	3.192 (6)	156.8

Symmetry code(s): (i) -x, -y, -z+1; (ii) -x+1, -y, -z+1; (iii) x-1, y, z; (iv) x, y, z-1; (v) x-1, y, z-1.

Table S7. Comparison of selected geometric parameters between IMPB, IMPC and analogous examples of (110)-oriented layered perovskites found in the literature.

Compound	symm.	T (K)	Δd x 10^{-4}	σ^2 (deg^2)	θ_{link} (°)	d_{intra} (Å)	Ref.
IMMHyPbBr$_4$	$P2/c$	358	8.3	13.7	167.3(4)	8.51	This
(IMPB)	$P2_1/c$	100	13.5	28.7	**147.51(6)**	**8.16**	work
IMMHyPbCl$_4$	$P2/c$	390	10.5	15.1	167.0(8)	8.19	
(IMPC)	$P2_1/c$	100	31.5	44.7	**143.48(6)**	**7.95**	
FA$_{1.5}$AA$_{0.5}$PbBr$_4$	$P2_1/c$	93	6.2	20.7	169.20(6)	8.65	**1**
TzGUAPbBr$_4$	$P2_1/c$	93	11.0	28.2	169.58(3)	8.61	**2**
IMTzPbBr$_4$	$Pbcm$	298	11.7	26.6	171.41(2)	9.46*	**3**
FAHEAPbBr$_4$	$P2/n$	150	13.7	14.8	177.96(4)	8.55	**4**
PYTzPbBr$_4$	$Pmc2_1$	173	10.2	6.5	179.2(3)	9.36	**1**
PYGUAPbBr$_4$	P-1	173	10.6	14.9	180	9.15	**1**
IMGUAPbBr$_4$	$P1$	93	7.4	16.2	180	9.33	**2**
N-MEDAPbBr$_4$	$P2_12_12_1$	100	7.6	24.5	151.71(4)	8.39	**5**
EDBEPbBr$_4$	$P2_1/c$	100	24.0	24	156.57(2)	8.89	**6**
MlaPbBr$_4$	$P2_1/c$	298	17.6	114.8	159.85(3)	10.21	**7**
EPZPbBr$_4$	Pc	293	77.4	46.1	160.0(3)	9.29	**8**
APIPbBr$_4$	$P2_1/c$	293	26.0	20.8	162.68(4)	8.45	**9**
AA$_2$PbBr$_4$	$P2_1/c$	173	30.5	26.1	164.97(2)	9.28	**3**
3APRPbBr$_4$	$P2_1/c$	250	35.2	43.6	171.20(3)	9.69	**10**
m-FA$_2$PbBr$_4$**	$P2_1/c$	100	21.4	70.3	172.94(3)	7.98	**11**
t-FA$_2$PbBr$_4$	P-1	100	4.8	31.2	177.3(1)	8.56	**11**
TMEDA$_{0.5}$DMAPbCl$_4$	$P2_1/c$	296	22.7	43.7	165.12(5)	8.89	**12**
APIPbCl$_4$	$P2_1/c$	298	13.7	16.7	167.70(9)	8.80	**13**
3APRPbCl$_4$	$P2_1/c$	298	12.3	34.5	169.7(1)	8.98	**10**
PPZPbCl$_4$	$P2_1/c$	293	2.1	32.2	174.10(1)	9.06	**14**

Δd – bond length distortion, σ^2 – octahedral bond angle variance, θ_{link} – Pb–X–Pb angles for the linking 'X' halogen, d_{intra} – distances between corresponding Pb atoms inside the octahedra layer, measured along [001] direction. In case of coexistence of inequivalent octahedra in one phase, larger Δd and σ^2, and smaller θ_{link} and d_{intra} values are provided in the table.

* – structure with 3x3 corrugation type of octahedra layers, distances between the middle Pb atoms were calculated.

** – m- and t- denote monoclinic and triclinic phase of FA$_2$PbBr$_4$.

IM = imidazolium, MHy = methylhydrazinium, FA = formamidinium, AA = acetamidinium, Tz = 1,2,4-triazolium, GUA = guanidinium, HEA = hydroxyethylammonium, PY = pyrazolium, *N*-MEDA = *N*-methylethane-1,2-diammonium, EDBE = 2,2′-(ethylenedioxy)bis(ethylammonium), Mla = melammonium, EPZ = 1-ethylpiperazine, API = *N*-(3-aminopropyl)imidazolium, 3APR = 3-aminopyrrolidinium, TMEDA = N,N,N′,N′-tetramethylethylenediammonium, DMA = dimethylammonium, PPZ = piperazinium.

References to Table S7

1 Y. Y. Guo, C. Elliott, J. A. McNulty, D. B. Cordes, A. M. Z. Slawin and P. Lightfoot, *Eur. J. Inorg. Chem.*, 2021, 3404–3411.

2 Y. Y. Guo, J. A. McNulty, N. A. Mica, I. D. W. Samuel, A. M. Z. Slawin, M. Bühl and P. Lightfoot, *Chem. Commun.*, 2019, **55**, 9935–9938.

3 Y. Y. Guo, L. J. Yang, S. Biberger, J. A. McNulty, T. Li, K. Schötz, F. Panzer and P. Lightfoot, *Inorg. Chem.*, 2020, **59**, 12858–12866.

4 M. B. H. Salah, N. Mercier, M. Allain, N. Zouari, U. Giovanella and C. Botta, *Eur. J. Inorg. Chem.*, 2019, 4527–4531.

5 E. R. Dohner, E. T. Hoke and H. I. Karunadasa, *J. Am. Chem. Soc.*, 2014, **136**, 1718–1721.

6 E. R. Dohner, A. Jaffe, L. R. Bradshaw and H. I. Karunadasa, *J. Am. Chem. Soc.*, 2014, **136**, 13154–13157.

7 W. Huang, X. Zhang, Y. Li, Y. Zhou, X. Chen, X. Li, F. Wu, M. Hong, J. Luo, S. Zhao, W. Huang, Y. Li, Y. Zhou, X. Chen, X. Li, F. Wu, M. Hong, J. Luo, S. Zhao and X. Zhang, *Angew. Chemie Int. Ed.*, 2022, **61**, e202202746.

8 L. Mao, P. Guo, M. Kepenekian, I. Hadar, C. Katan, J. Even, R. D. Schaller, C. C. Stoumpos and M. G. Kanatzidis, *J. Am. Chem. Soc.*, 2018, **140**, 13078–13088.

9 Y. Y. Li, C. K. Lin, G. L. Zheng, Z. Y. Cheng, H. You, W. D. Wang and J. Lin, *Chem. Mater.*, 2006, **18**, 3463–3469.

10 X. Li, P. Guo, M. Kepenekian, I. Hadar, C. Katan, J. Even, C. C. Stoumpos, R. D. Schaller and M. G. Kanatzidis, *Chem. Mater.*, 2019, **31**, 3582–3590.

11 S. A. Fateev, A. A. Petrov, E. I. Marchenko, Y. V. Zubavichus, V. N. Khrustalev, A. V. Petrov, S. M. Aksenov, E. A. Goodilin and A. B. Tarasov, *Chem. Mater.*, 2021, **33**, 1900–1907.

12 Y. Y. Ma, H. M. Pan, D. Y. Li, S. Wu and Z. Jing, *Zeitschrift für Anorg. und Allg. Chemie*, 2022, **648**, e202100334.

13 Z. Wu, C. Ji, Z. Sun, S. Wang, S. Zhao, W. Zhang, L. Li and J. Luo, *J. Mater. Chem. C*, 2018, **6**, 1171–1175.

14 A. Bonamartini Corradi, A. M. Ferrari, L. Righi and P. Sgarabotto, *Inorg. Chem.*, 2001, **40**, 218–223.
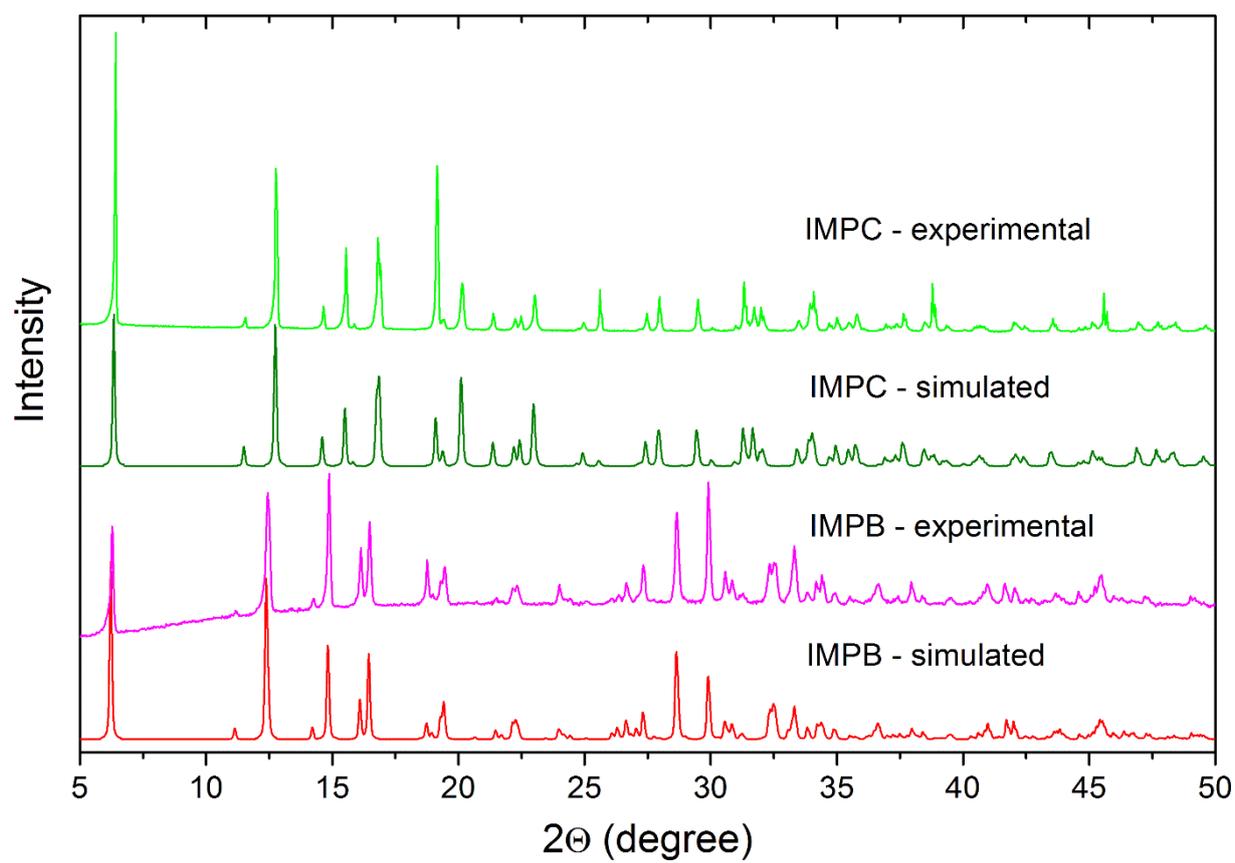
**Figure S1**. RT X-ray diffraction patterns for the obtained samples together with the calculated ones based on the RT single crystal data.
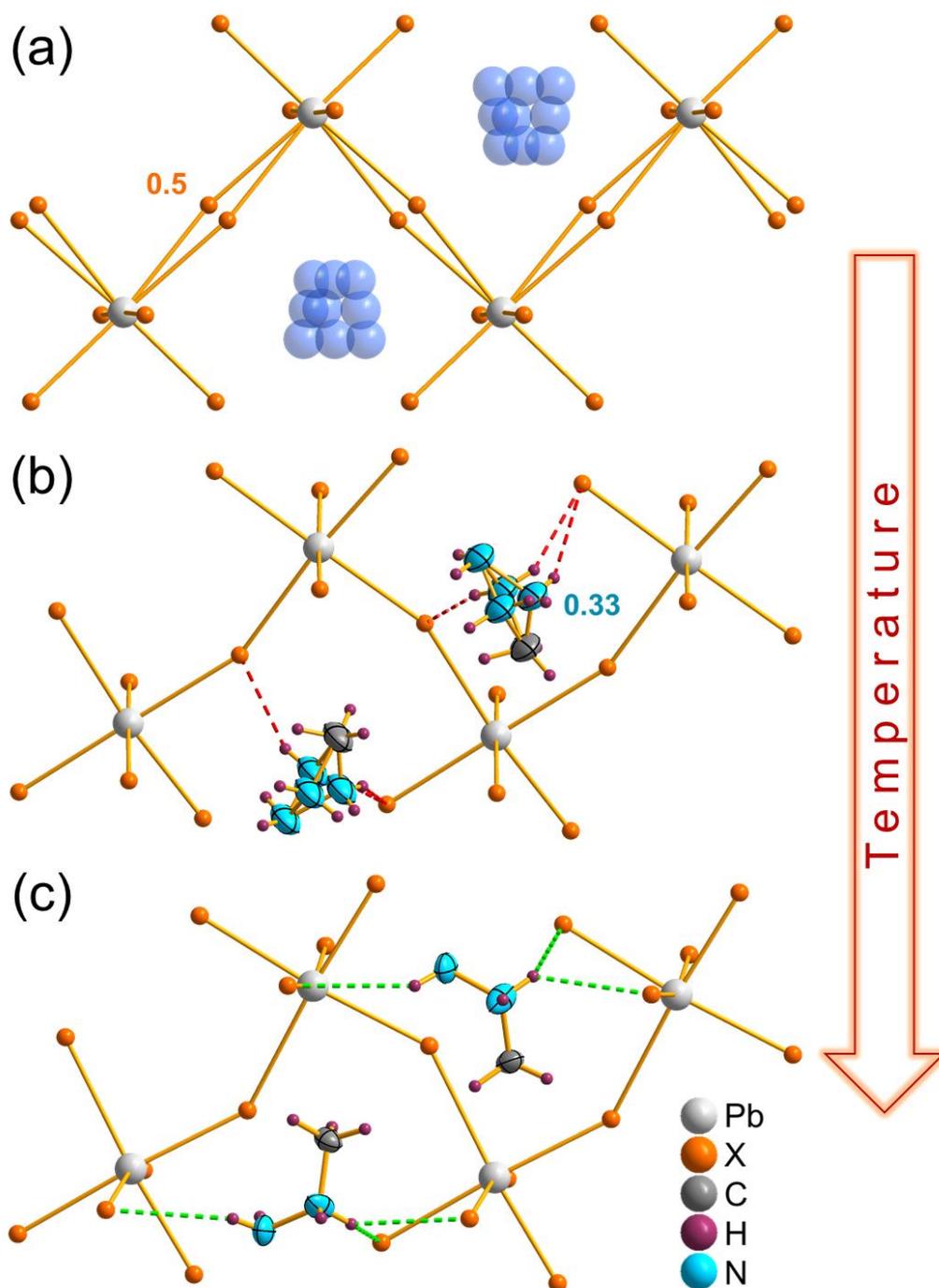
Figure S2. Changes in geometry of single layer of $[PbX_6]_\infty$ octahedra (X = Br, Cl) and dynamics of intra-layer MHy$^+$ cation in: (a) phase **I** (*P*2/*c*) with the linking halide split into two symmetrically equivalent positions with equal occupancy and heavily disordered MHy$^+$, (b) phase **II** (*P*2$_1$/*c*) at 295 K with ordered halides and still disordered the middle N atom of MHy$^+$ which is split into three symmetrically inequivalent positions with equal, 1/3 probability and (c) phase **II** (*P*2$_1$/*c*) at 100 K with all atoms ordered. Red dashed lines in (b) denote potential hydrogen bonding between disordered N atom of MHy$^+$ with X$^-$ acceptors. Green dashed lines in (c) represent N–H···X HBs.
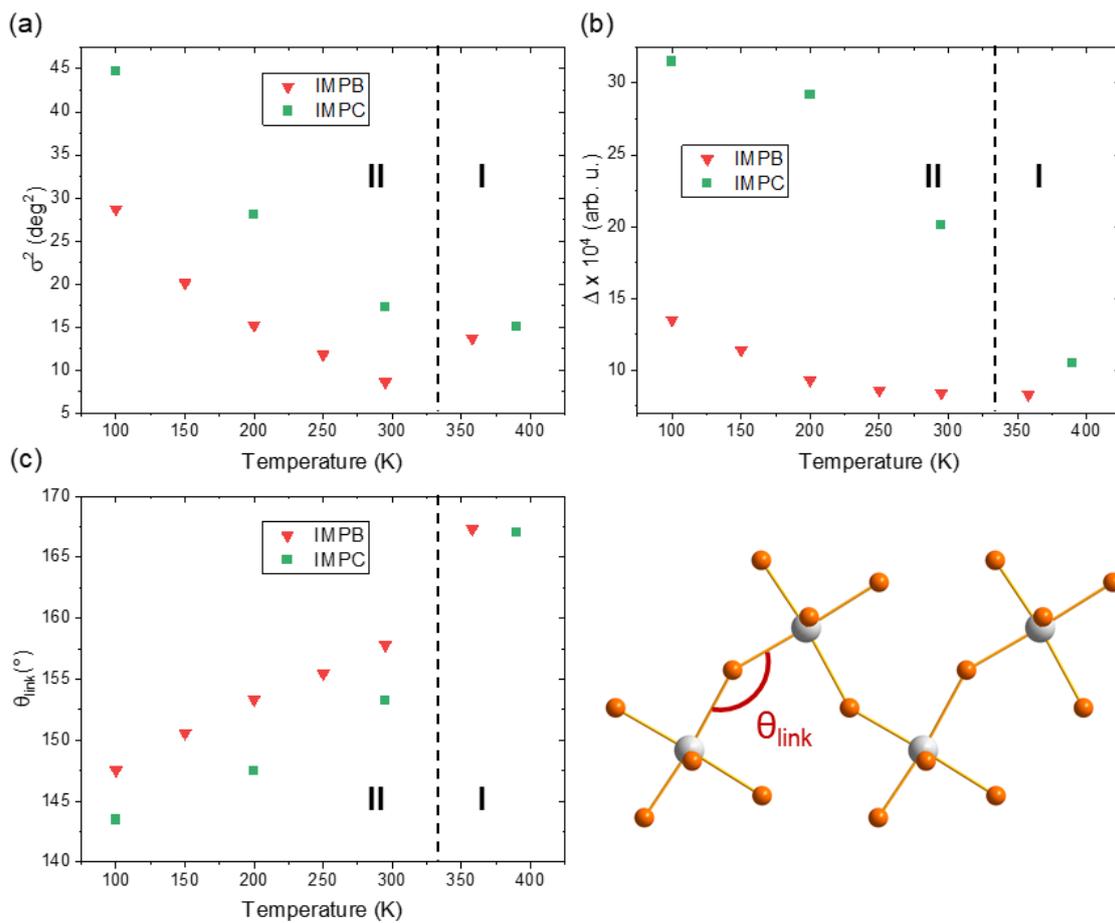
Figure S3. The temperature dependence of the (a, b) octahedral distortion parameters – (a) octahedral bond angle variance (σ^2) and (b) bond length distortion (Δd), and (c) Pb–X–Pb angles for the linking 'X' halogen (θ_{link}). **I** and **II** correspond to phase **I** (*P2/c*) and phase **II** (*P2₁/c*), respectively.
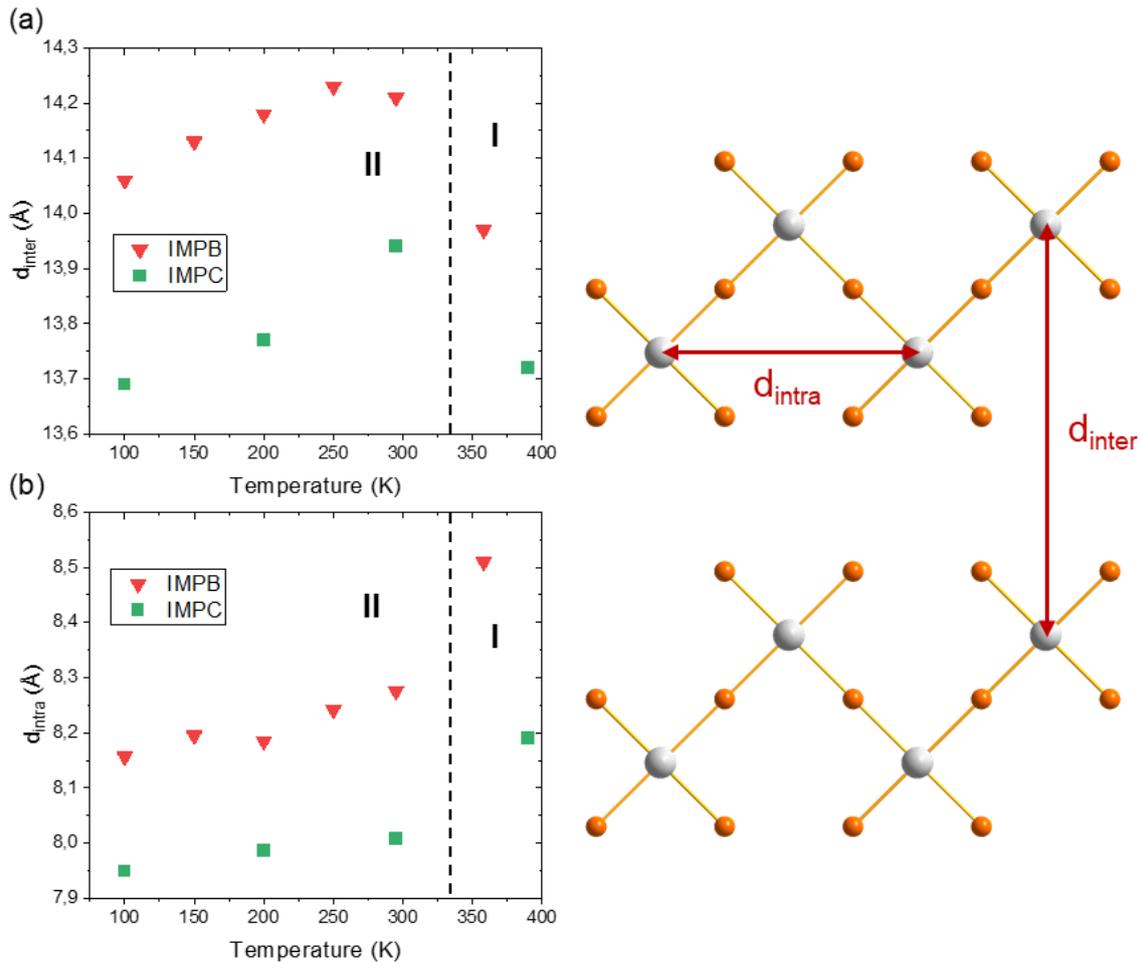
Figure S4. Distances between corresponding Pb atoms of (a) neighbouring layers (d_{inter}) and (b) inside the layers measured along [001] direction (d_{intra}) as a function of temperature. **I** and **II** correspond to phase **I** ($P2/c$) and phase **II** ($P2_1/c$), respectively.
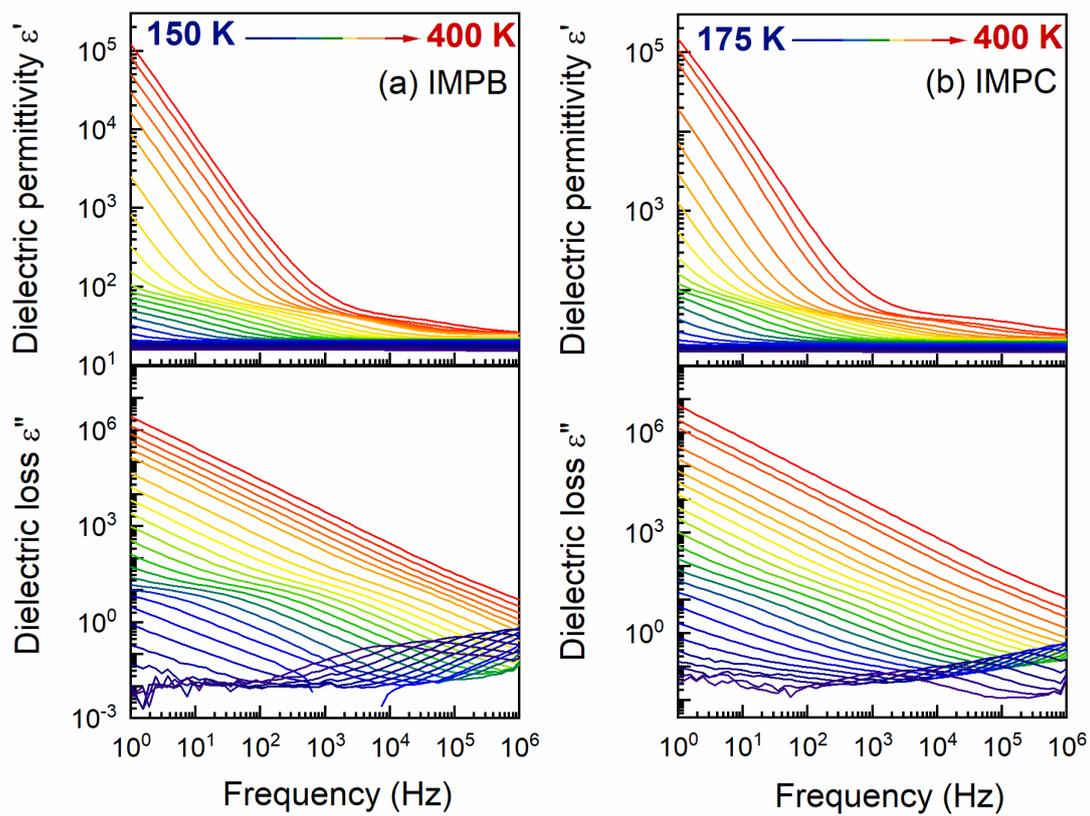
Figure S5. Frequency dependence of complex dielectric spectra for two samples in the temperature range from 150 (175) K to 400 K for (a) IMPB and (b) IMPC, respectively.
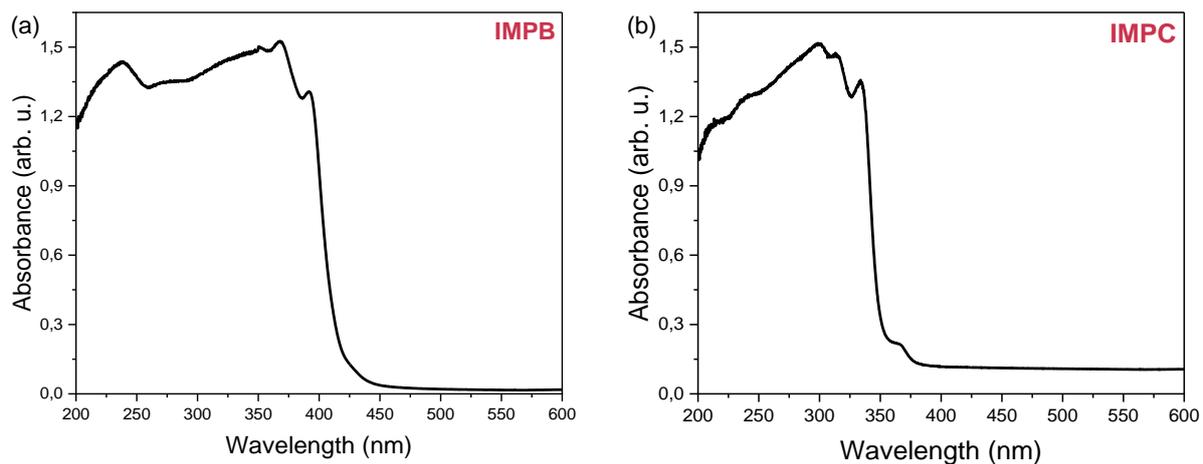
Figure S6. Diffuse-reflectance spectra (DRS) of (a) IMPB and (b) IMPC.
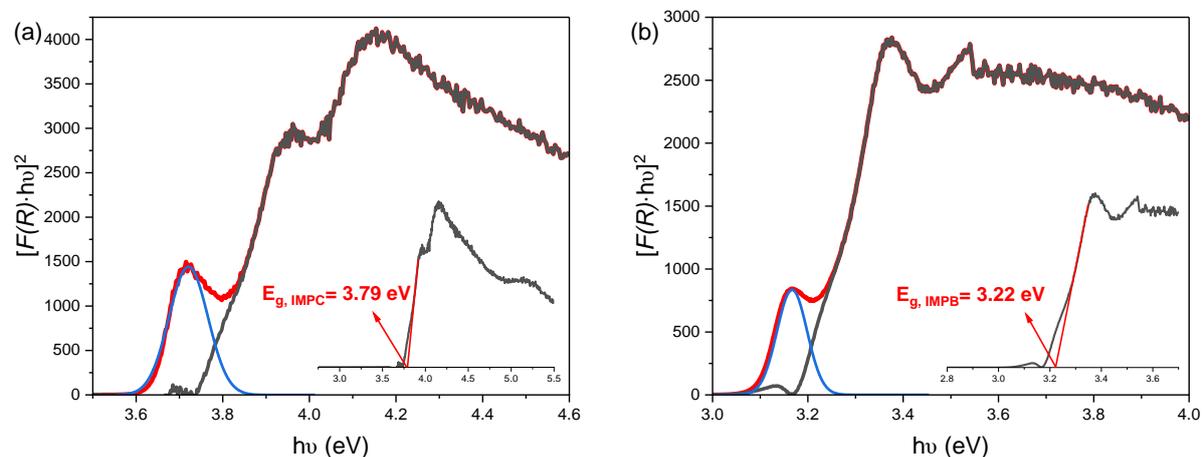
Figure S7. Kubelka-Munk functions (red lines) for (a) IMPB and (b) IMPC with Gauss fit of free exciton peaks (blue lines), the Kubelka-Munk functions after exciton peak subtraction (black lines) as well as band gap (E_g) estimation with Tauc plots (inserts).
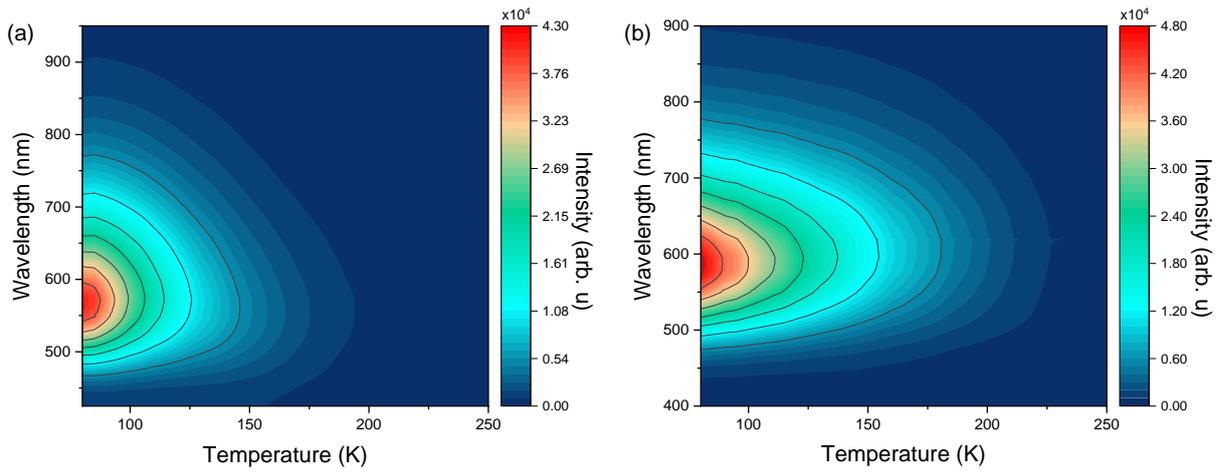
**Figure S8.** Maps of the thermal evolution of emission for: (a) IMPB and (b) IMPC.
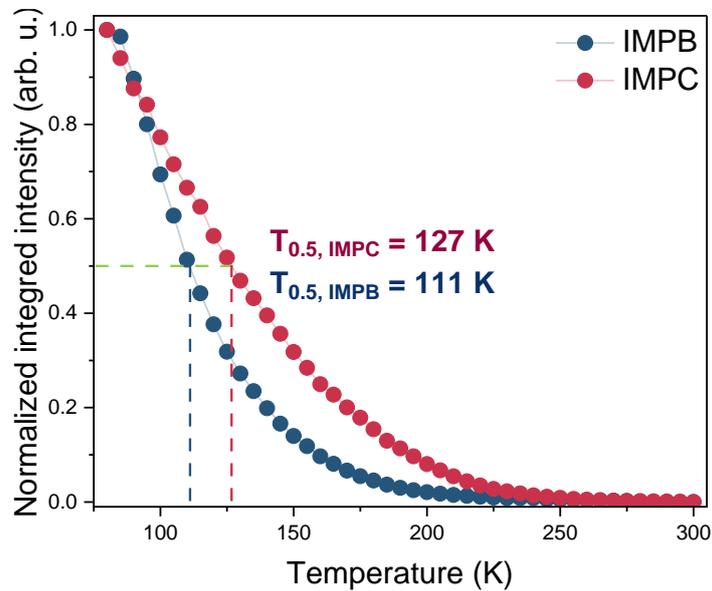
Figure S9. Determination of $T_{0.5}$ parameters for IMPB and IMPC.
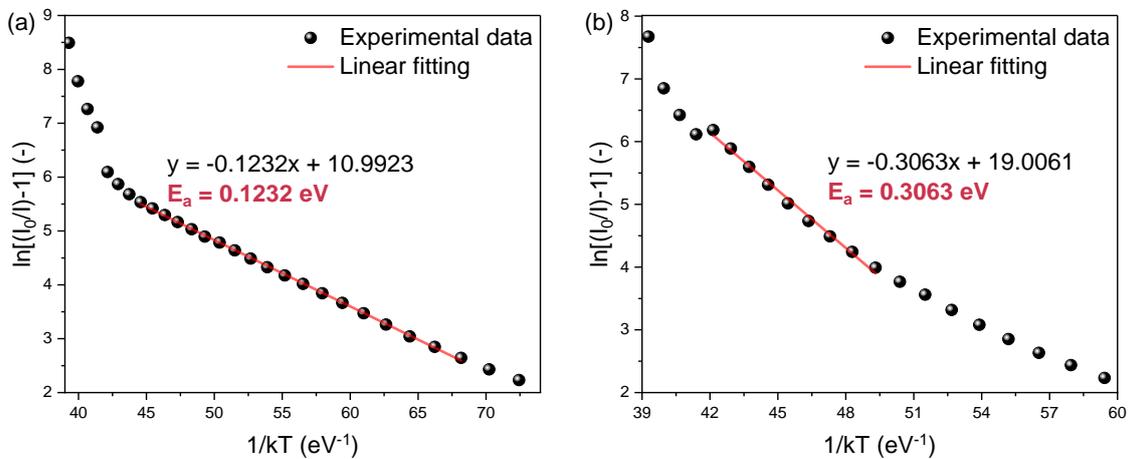

Figure S10. Determination of the energy activation of thermal quenching for: (a) IMPB and (b) IMPC.